Heterogeneous Ice Nucleation in Aqueous Solutions: the Role of Water Activity

B. Zobrist,[†,‡] C. Marcolli,[†] T. Peter,[†] and T. Koop*[,‡]

Institute for Atmospheric and Climate Science, ETH Zurich, Zurich, Switzerland, and Department of Chemistry, Bielefeld University, D33501 Bielefeld, Germany

Received: November 27, 2007; In Final Form: February 6, 2008

Heterogeneous ice nucleation experiments have been performed with four different ice nuclei (IN), namely nonadecanol, silica, silver iodide and Arizona test dust. All IN are either immersed in the droplets or located at the droplets surface. The IN were exposed to various aqueous solutions, which consist of $(NH_4)_2SO_4$, H_2SO_4, $MgCl_2$, NaCl, LiCl, $Ca(NO_3)_2$, K_2CO_3, CH_3COONa, ethylene glycol, glycerol, malonic acid, PEG300 or a NaCl/malonic acid mixture. Freezing was studied using a differential scanning calorimeter and a cold finger cell. The results show that the heterogeneous ice freezing temperatures decrease with increasing solute concentration; however, the magnitude of this effect is solute dependent. In contrast, when the results are analyzed in terms of the solution water activity a very consistent behavior emerges: heterogeneous ice nucleation temperatures for all four IN converge each onto a single line, irrespective of the nature of the solute. We find that a constant offset with respect to the ice melting point curve, $\Delta a_{w,het}$, can describe the observed freezing temperatures for each IN. Such a behavior is well-known for homogeneous ice nucleation from supercooled liquid droplets and has led to the development of water-activity-based ice nucleation theory. The large variety of investigated solutes together with different general types of ice nuclei studied (monolayers, ionic crystals, covalently bound network-forming compounds, and a mixture of chemically different crystallites) underlines the general applicability of water-activity-based ice nucleation theory also for heterogeneous ice nucleation in the immersion mode. Finally, the ice nucleation efficiencies of the various IN, as well as the atmospheric implication of the developed parametrization are discussed.

1. Introduction

Water is involved in numerous biological and geophysical processes. Ice, liquid water and water vapor can all be stable at atmospheric pressures and temperatures, but they exhibit vastly different physical properties. Hence, phase transitions between the states of water distinctly alter the attributes of a particular system. For example, in the atmosphere, the light scattering properties of liquid and solid cloud particles differ significantly with implications for the Earth's radiative budget.[1] As another example, in the biosphere, ice formation in cell fluid of organisms may be lethal, because ice growth can destroy the cell membranes.[2]

The first step of the transition from water to ice is the formation of minuscule ice-like clusters inside the liquid phase, due to fluctuations within the liquid. Once the size of such a cluster exceeds a critical value, it grows spontaneously to form an ice crystal of macroscopic size. This stochastic process is called homogeneous ice nucleation and occurs in water or aqueous solutions devoid of foreign particles or substrates.[3] On the other hand, ice nucleation can occur at the surface of so-called ice nuclei (IN) in what is termed a heterogeneous nucleation process. It has been argued that heterogeneous ice nucleation is predominant in biological systems,[4] where it occurs at the surface of special proteins acting as ice nucleation agents.[5,6] One distinguishes four principal modes of how heterogeneous ice nucleation may take place:[7] contact freezing, deposition nucleation, condensation freezing and immersion freezing. Modeling studies suggest that deposition nucleation and immersion freezing are the most important heterogeneous ice nucleation modes at cirrus cloud temperatures.[8,9] In the present study we focus on immersion freezing, where ice nucleation occurs at the surface of an ice nucleus immersed in water or in an aqueous solution. Note that the physical process behind ice nucleation induced by a surfactant monolayer can be put on par with immersion mode freezing as described in the textbook by Pruppacher and Klett.[3] This is due to the fact that the surfactant surface is completely wetted by the liquid aqueous phase, which is a prerequisite for immersion mode freezing. Therefore, in this study we use the term immersion mode also for ice nucleation in the liquid beneath a surfactant monolayer.

It is well-established that homogeneous ice freezing temperatures decrease with increasing solution concentration and that this decrease can be described as a function of water activity of the solution, irrespective of the nature of the solute.[10] Recent laboratory studies have started to investigate whether such a relationship also holds for heterogeneous ice nucleation in the immersion mode. These studies comprise different IN such as silicates,[11,12] metal oxides[12] or organic compounds[13,14] but were usually restricted to a single or very few solutes. In the present study, we investigate a larger variety of solutes and a broad range of IN to obtain a more general view on heterogeneous ice nucleation in the immersion mode.

Organic and inorganic IN have been investigated (i.e., nonadecanol monolayers, silver iodide crystals, silica spheres and Arizona test dust), all exhibiting different physical and chemical surface properties. Nonadecanol molecules form a

* To whom correspondence should be addressed. E-mail: thomas.koop@uni-bielefeld.de.
† ETH Zurich.
‡ Bielefeld University.

10.1021/jp7112208 CCC: $40.75
Published on Web 03/26/2008

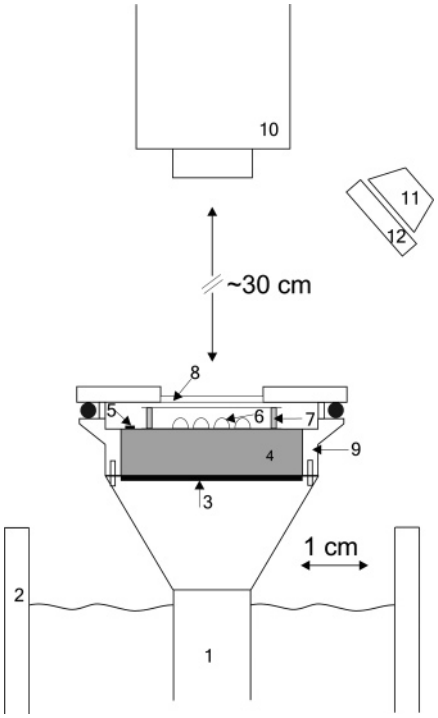

Figure 1. Schematic picture of the cold finger cell: 1, copper rod; 2, dewar filled with liquid nitrogen; 3, heating foil; 4, gold-coated copper block; 5, Pt100 temperature sensor; 6, droplets; 7, small cell containing the droplets; 8, glass window; 9, flange; 10, digital camera; 11, halogen lamp; 12, water tank.

flexible Langmuir monolayer with a 2D crystalline structure exhibiting a good structural match with ice.[15,16] In contrast, the other IN provide 3D structures with rigid surfaces. Arizona test dust is composed of silicates and metal oxides, whereas the other three IN consist of a single chemical compound. The investigated aqueous solutions are composed of various organic (e.g., malonic acid, ethylene glycol) or inorganic solutes (e.g., ammonium sulfate, sodium chloride) or mixtures of both (e.g., malonic acid/sodium chloride).

2. Experimental Section

The experiments were performed with an optical and a calorimetric device. The two setups combined allow the investigation of droplets with radii varying from a few microns up to 1 mm at temperatures from 150 to 293 K.

2.1. Cold Finger Cell. The cold finger cell detects freezing and melting of single droplets optically. The device is shown schematically in Figure 1. It consists of a cooling cell connected with a cold finger, a digital camera (C-Cam ccf15, resolution: 512 × 512 pixel) with an external light source (commercial halogen lamp), a temperature controller (Neocera, LTC-11) and a computer to control the experiment and to record the data. The entire setup is operated by a Labview user interface on the computer, to which the LTC-11 and the C-Cam are connected via a RS232 and a LVDS interface, respectively. An IR filter, made of a small water tank (12), is placed in front of the halogen lamp (11) to avoid any uncontrolled heating of the cooling cell by the light source.

The central part of the entire setup is the cooling cell. The small sample cell (7) inside the cooling cell consists of a silanized (hydrophobic) glass substrate, on which up to 6 droplets (6) can be placed. The cell is sealed by a cap, which is made of an O-ring covered by a second glass plate. It is placed onto a large gold-coated copper block (4), which is embedded and sealed by a flange (9). For optical detection, a glass window (8) is inserted in the top part of the flange. A large copper rod (1) is placed in a dewar filled with liquid nitrogen (2). The flange and the copper rod are connected via a cylindrical aluminum rod. The temperature of the copper block is controlled through a combination of constant cooling by the liquid nitrogen and heating by a heating foil (3; Minco HK 5561R37.4L12A) mounted below the copper block. A Pt100 temperature sensor (5) is attached to the copper block and connected to the temperature controller. This setup allows for control of the copper blocks temperature and, therefore, of the small cell, in the range 180−300 K using moderate cooling rates of 3 K min^{-1} and heating rates of 2 K min^{-1}. The absolute temperature calibration of the cooling cell is performed with the melting points of several organic substances (tetradecane, dodecane, decane and octane, all substances Fluka, puriss.) and the ice melting points of aqueous $(NH_4)_2SO_4$ (Sigma, 99.99+%) and (Merck, p.a.) solutions; all aqueous solutions in this work were made with distilled and deionized water (Resistivity ≥18.2 MΩ cm). This calibration leads to an accuracy of the freezing and melting points of ±0.4 K. Under the present experimental conditions, the cold finger cell allows the investigation of droplets with radii larger than 500 μm.

2.2. Differential Scanning Calorimeter (DSC). A commercial differential scanning calorimeter (DSC, TA Instruments Q10) with a LNCS cooling system was used in this study. This setup allows for the determination of the phase transition temperatures in the range between 130 and 600 K with a precision of ±0.01 K. The cooling and heating rates can be adjusted between 0.01 and 50 K min^{-1}, but we used mainly cooling and heating rates of 10 and 1 K min^{-1}, respectively. The DSC sample pan can be loaded with bulk samples (single droplets with a volume of several microliters) or emulsified samples. A 20−30 mg sample of an emulsion was used in an experiment, which corresponds to approximately 10^7 aqueous droplets. An empty DSC pan is always used as the reference sample. The DSC temperature calibration was performed using the melting point of ice and the ferroelectric phase transition of $(NH_4)_2SO_4$ at 223.1 K.[17] The accuracies of the reported freezing and melting points are ±0.5 and ±0.3 K, respectively. The freezing temperature was determined as the onset point of the freezing peak (i.e., intersection of the tangent drawn at the point of greatest slope at the leading edge of the thermal peak with the extrapolated baseline), whereas the melting point temperature was determined as the maximum of the ice melting peak.

2.3. Preparation of Ice Nuclei and Typical Experiments. ***2.3.1. Nonadecanol.*** In several previous studies it was shown that long chain alcohols located at the air/water interface of aqueous solution or water droplets are highly potent IN,[14−16,18,19] with heterogeneous freezing temperatures up to 272 K.[15] In contrast, a water droplet of the same size with no alcohol coating would freeze homogeneously at ∼242 K.[3] In this study, the droplets covered by a monolayer of nonadecanol ($C_{19}H_{39}OH$) have been investigated with the cold finger cell. In each experimental run, six 3 μL aqueous solution droplets (i.e., radius ≈1100 μm) were placed on a silanized (hydrophobic) glass substrate. The nonadecanol monolayer was prepared by spreading 0.5 μL of a 2.5 × 10^{-4} M 1-nonadecanol (Fluka, purum)/hexane (Fluka, puriss.) solution onto the droplets using a micropipet. After the hexane had evaporated (within a few seconds), the droplets were sealed inside the small cell (see Figure 1). The utilized amount of nonadecanol is sufficient to produce a monolayer with a surface area that is a factor of 1.5

larger than that of the droplet. Five freezing/melting cycles were investigated for each set of six droplets. The samples were always cooled with a rate of 3 K min^{-1} until freezing was observed. Subsequently the samples were heated at a rate of 2 K min^{-1} to 285 K. Note that the ice nucleation of droplets covered by nonadecanol is indeed induced by nonadecanol and is not affected by traces of hexane. In separate experiments without hexane but with nonadecanol at the interface between water and a mineral oil phase[19] practically the same freezing temperatures were observed, suggesting that neither oil nor hexane play a significant role in ice nucleation. In addition, it has been shown in previous independent experiments that ice nucleation does not start preferentially at the air/water/glass triple junction but is evenly distributed over the whole monolayer interface, in agreement with our treatment.[20]

In total, 15 solutions were investigated with the following compositions: pure water; 5.6, 15.0, 23.9 and 34.2 wt % $(NH_4)_2SO_4$; 6.9, 17.1 and 19.6 wt % $MgCl_2$ (Fluka, ≥99%); 15.1 and 19.9 wt % NaCl; 29.8 and 43.8 wt % $Ca(NO_3)_2$ (Fluka, purum); 30.0, 42.9 and 48.1 wt % ethylene glycol (Fluka, ≥99.5%).

2.3.2. Silica (SiO_2). We applied a method developed by Stöber et al.[21] to synthesize nanometer-sized silica spheres with a narrow size distribution. This method uses tetraethylorthosilicate (TEOS) in the presence of a $C_2H_5OH/NH_3/H_2O$ mixture. The size of the particles depends on the ratio between the NH_3 and H_2O concentrations, with smaller ratios producing smaller particles.[22] Our goal was to achieve a radius of ∼100 nm. Therefore, the following four ingredients were added one after the other to a 500 mL glass flask: 188 mL of C_2H_5OH (Fluka, pure), 7 mL of H_2O (distilled and deionized water, 18.2 MΩ cm), 7 mL of a 25% NH_3/H_2O solution (Fluka, standard solution) and 8 mL of TEOS (Fluka, 99.9999%). This mixture was stirred with a magnetic stirrer for 18 h at room temperature. Thereafter, the precipitated nanometer-sized silica spheres were isolated from the solvent mixture by centrifugation. The resulting colorless powder was placed in an oven at 100 °C for 16 h and weighed afterward. After the particles were placed again in the oven for 4 h, it was found that the mass of the particles remained constant, indicating that H_2O, C_2H_5OH or NH_3 had been evaporated during this procedure. The mean diameter of the silica spheres was determined with a scanning electron microscope (Zeiss Gemini 1530 FEG) to be about 90 nm with a standard deviation of 20 nm.

A silica/water stock suspension together with various solutes were used to prepare aqueous solutions containing silica spheres. The silica mass fraction in each of these solutions was 0.47% of the total water mass, which is equivalent to about 10^9-10^{10} silica spheres in a 3 μL sample (a density of 2 g cm^{-3} for the silica particles is assumed). Before each experiment, the suspensions were placed in an ultrasonic bath for 10 min to decrease particle aggregation. Droplets with a volume of 3 μL, i.e., radius of ≈1100 μm, were placed in a DSC pan and sealed by a cover and vacuum grease to prevent any water evaporation during the experiment. The samples were cooled at 10 K min^{-1} and heated at 1 K min^{-1}. Four freezing/melting cycles were performed for each droplet and at least two independent droplets were investigated for each aqueous solution. The investigated droplets had the following solute composition: pure water; 7.7, 15.7, 25.4, 32.7 and 39.0 wt % $(NH_4)_2SO_4$; 14.9 wt % LiCl (Aldrich, ≥99%); 10.8 wt % H_2SO_4 (Merck, p.a.).

2.3.3. Silver Iodide (AgI). Silver iodide (AgI) crystallites were prepared in-situ within emulsion droplets by a precipitation reaction similar to that by Aguerd et al.[23] First, 0.1 mL of a 1.64 wt % $AgNO_3$ (Sigma, ≥99%) solution, 1.6 mL of a 23 wt % lanolin (Fluka) in mineral oil (Aldrich) mixture and 0.1 mL of a 1.61 wt % KI (Fluka, ≥99%) solution were added one after the other to a test tube. This mixture was stirred with a commercial drilling machine at 7000 rpm for 5 min, leading to the precipitation of AgI crystallites within the emulsion droplets. Then 0.4 mL of an aqueous solution of a particular solute (e.g., 2 wt % $LiCl_2$ solution) was added and the entire mixture stirred for another 15 min. This preparation procedure resulted in emulsion droplets with a mean diameter of 3 μm with a standard deviation of 2 μm consisting of an aqueous solution mixture of KNO_3, the additional solute, and AgI crystallites. To change the surface area of the AgI crystallites per droplet, the mass of $AgNO_3$ and was reduced by a factor of 2 in some experiments. This reduction decreases the AgI surface area by a factor of ∼1.5 (≈$2^{2/3}$, assuming only one AgI crystallite per droplet).

All experiments with emulsions containing AgI crystallites were performed with the DSC. At least two individual freezing/melting cycles with cooling and heating rates of 10 and 1 K min^{-1}, respectively, have been performed for each sample solution. The investigated solutions were: pure water; 2.0, 7.7, 14.9 and 19.9 wt % LiCl; 17.9 and 39.5 wt % K_2CO_3 (Fluka, ≥99%); 13.0, 29.8 and 43.9 wt % $Ca(NO_3)_2$; 3.0, 9.0, 17.1, 22.5 and 25.0 wt % $MgCl_2$; 19.5 and 28.3 wt % CH_3COONa (Fluka, ≥99%); 21.4 and 29.9 wt % ethylene glycol; 39.6 wt % glycerol (Fluka, ≥99.5%).

2.3.4. Arizona Test Dust (ATD). Commercially available ultra fine Arizona test dust (ATD, Powder Technology Inc.) with a nominal particle diameter between 0 and 3 μm was used for the ice nucleation experiments. The size distribution of such ATD particles has been determined in a recent study.[24] To achieve emulsions with immersed ATD particles, four parts of a 5 wt % lanolin in mineral oil mixture and one part of a 5 wt % ATD aqueous solution suspension were stirred by a rotor-stator homogenizer (Polytron PT 1300 D with a PT-DA 1307/2EC dispersing aggregate) for 40 s at 7000 rpm. The resulting droplet size distribution of the emulsion can be described by a normal distribution with a median diameter of 10.0 μm and variance of 14.8.[24] Two freezing/melting cycles (cooling rate, 10 K min^{-1}; heating rate, 1 K min^{-1}) have been performed for each emulsion. Besides 5 wt % of dispersed ATD, the investigated solutions contained the following solutes: pure water; 4.8, 10.2, 19.6 and 30.0 wt % $(NH_4)_2SO_4$; 5.9 wt % NaCl; 5.1 wt % H_2SO_4; 10.5, 25.1 and 39.8 wt % malonic acid (Fluka, ≥99%); 11.0 wt % poly(ethylene glycol) 300 (Aldrich, with a number average molar mass of 306 g mol^{-1}); 4.1/8.3 wt % NaCl /malonic acid.

3. Results and Discussion

First, the experiments with each IN are discussed individually, and second, combined data sets are examined. All data are listed in Tables 1−4 in Appendix A.

3.1. Characteristics of Experiments with Individual IN. ***Large Droplets Covered by Nonadecanol Monolayers.*** Up to 18 individual droplets for each of a total of 15 different aqueous solutions have been investigated using the cold finger cell. In all experiments the heterogeneous freezing temperature in the first freezing cycle was 6−10 K lower than those of the subsequent cycles. Such a behavior has also been described for droplets covered by other long chain alcohols.[14,18,19] Seeley and Seidler[18] attributed this phenomenon to a possible pre-activation mechanism of such monolayers, resulting from different start temperatures of the cycles. In the present study, the first cycle started at 294 K, whereas the subsequent cycles all started at

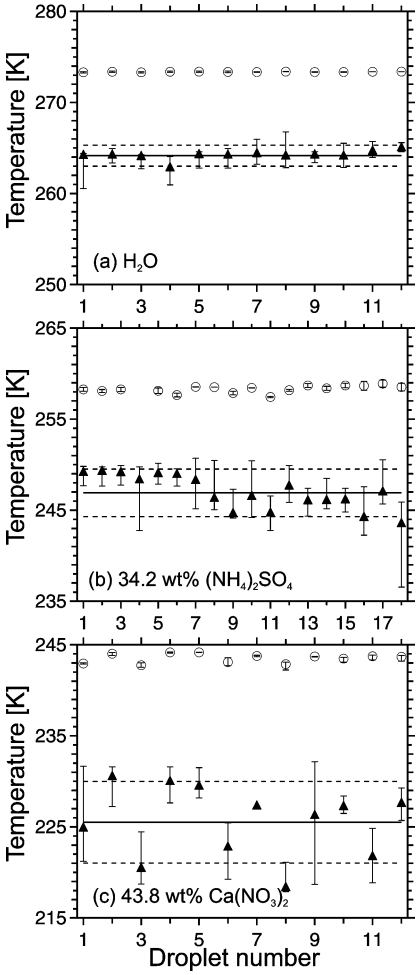

Figure 2. Median heterogeneous ice freezing temperatures (filled triangles) and mean ice melting temperatures (open circles) with error bars of four freezing and melting cycles for individual droplets covered by nonadecanol: (a) H_2O; (b) 34.2 wt % $(NH_4)_2SO_4$; (c) 43.8 wt % $Ca(NO_3)_2$. The error bars indicate the maximum deviation of a freezing or melting point from the corresponding median or mean value, respectively. Solid lines: mean value of the median freezing temperatures. Dotted-lines: ±one standard deviation (of all single freezing temperatures) around the solid line.

285 K. Therefore, the first heterogeneous freezing temperature in each experiment was not considered for further analysis. The freezing points of water droplets covered by nonadecanol agree well with the measurements by Gavish et al.[15] They reported that 10−40 μL droplets exhibit an average heterogeneous freezing temperature of ∼266 K with a standard deviation of about 1 K, in comparison to 264.2 and 1.2 K for 3 μL droplets observed in this study.

Figure 2 shows median heterogeneous ice freezing and mean ice melting points for 12 to 18 identically prepared droplets of three different aqueous solutions. The three cases shown in Figure 2 comprise the data with the smallest (pure water) and largest (43.8 wt % $Ca(NO_3)_2$) scatter in the heterogeneous ice freezing temperatures. For an individual droplet, heterogeneous ice freezing points generally exhibit a larger scatter than the ice melting points, as is expected on the basis of the stochastic nature of the nucleation process. The variation of the freezing temperatures between different droplets increases with increasing solution concentration. The maximum difference between the lowest and the highest freezing temperature was 3.9 K in the case of pure water (droplet 8 in Figure 2a) compared with 14.0 K for a 43.8 wt % $Ca(NO_3)_2$ solution droplet (droplet 9 in Figure 2c). The standard deviation of all freezing points, shown in Figure 2 as dashed lines, increases from 1.2 K (pure water) over 2.6 K (34.2 wt % $(NH_4)_2SO_4$) up to 4.5 K for the 43.8 wt % $Ca(NO_3)_2$ droplets. Most median freezing temperatures for an individual droplet series are within the temperature range bounded by the dashed lines. The few exceptions (e.g., droplet 8 for the 43.8 wt % $Ca(NO_3)_2$ solution) may be caused by a change in concentration of the droplets due to water evaporation during the experiment and, thus, such series would compare unequal droplets. Ten out of 132 melting point series exhibit difference between the highest and lowest value larger than 0.8 K (±0.4 K for the melting calibration), indicating that the concentration of the droplets may have changed during the experiment. In Figure 2, this is observed for droplets 16 and 18 of the 34.2 wt % $(NH_4)_2SO_4$ solution and for droplets 6 and 8 of the 43.8 wt % $Ca(NO_3)_2$ solution. Partial evaporation of water from the droplets is supported by the fact that 9 of these 10 cases show a continuous decrease in the melting point with increasing experimental time. Evaporation was typically observed just in one of the six droplets investigated in an experiment, indicating that this issue is not a general limitation of the cold finger cell, but rather a problem of individual droplets. Experimental considerations give evidence that a droplet with an uncomplete monolayer evaporates distinctly faster than a fully covered droplet. Hence the ten series that exceed a maximum difference in the melting point are most likely not fully covered with nonadecanol. Because evaporating and nonevaporating droplets can be clearly distinguished from the melting point analysis, we believe that no systematic bias in the data is introduced.

Note that water evaporation was observed only for the most highly concentrated solutions, in which a small amount of water evaporation results in a larger change in the melting point temperature because of the much steeper concentration dependence of the ice melting point curve at high concentrations. Hence the 10 series, which exceed a maximum difference in the melting point are most likely not fully covered with nonadecanol. In general, no correlation between the largest difference in the freezing temperatures and the largest difference in the melting temperatures was observed. For example, droplet 9 of the 43.8 wt % $Ca(NO_3)_2$ solution shows the largest difference in the freezing temperatures of 14.0 K, but the difference in the melting points is only 0.08 K. Therefore, the large difference between the freezing points in this particular case must result from reasons other than concentration changes of the droplets. Apart from the stochastic nature of the nucleation process also structural changes in the monolayer may influence the freezing efficiency and, hence, might be an explanation for this observation.[14,19] However, further experiments are required to verify the latter suggestion.

Large Droplets Containing Silica Spheres. Water droplets (3 μL) containing silica spheres placed in an aluminum DSC pan froze at around 255 K. This is close (but not identical) to the freezing temperature of 3 μL water droplets without silica spheres in the DSC pan ($T_f \approx 252-253$ K), but much higher than the homogeneous freezing temperature of pure water droplets of the same size, which is about 242 K according to classical nucleation theory.[3] Freezing in those droplets without silica spheres was most likely initiated at the Al_2O_3 surface of the DSC sample pans. We have shown in a previous study,[19] that the Al_2O_3 surface can act as an ice nucleus. Therefore, in the present study we had to distinguish whether the nucleation process in the investigated droplets with silica spheres was induced by the DSC pan surface or by the silica spheres. Hence, for each investigated aqueous solution sample containing silica

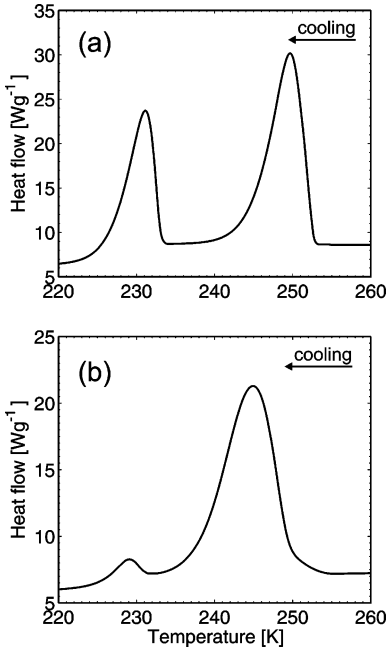

Figure 3. DSC thermograms as a function of temperature for two emulsified samples: (a) 2.0 wt % LiCl aqueous solution containing precipitated AgI crystallites; (b) 11.0 wt % PEG300 aqueous solution containing immersed ATD particles.

spheres, we also investigated the freezing temperature of eight samples with the same concentration but without silica spheres for comparison. The dissimilarity of two such data sets was then determined by a Wilcoxon rank sum test on the 5% level.[25] Only one data series did not pass this test and, hence, was not used for further evaluation.

The scatter in freezing temperature was less than 5 K for all series. The ice melting points differed from each other by less than the calibration uncertainty, indicating that the concentration of the droplets remained constant during the experiments.

Emulsions Containing Immersed AgI Crystallites. Figure 3a shows a DSC cooling thermogram of an emulsion containing AgI crystallites. Two freezing signals at different temperatures were observed. The first (high temperature) signal is assigned to heterogeneous ice freezing induced by AgI, whereas the second (low temperature) signal corresponds to homogeneous ice freezing of those droplets that do not contain AgI crystallites. Thus, the thermogram indicates that not all emulsion droplets contain an ice nucleus. The homogeneous and heterogeneous freezing temperatures in this study vary by less than 2 K between different cooling cycles of the same emulsion. The ice melting points differ by less than the calibration uncertainty.

The amount of the $AgNO_3$ and KI solutions was reduced by a factor of 2 in some experiments, which decreases the AgI surface area by a factor of ~1.5. The difference in the heterogeneous freezing temperatures between experiments with normal and reduced $AgNO_3$ and concentrations was less than 0.2 K and the ratio between the heterogeneous to homogeneous peak sizes did not change. This indicates that a moderate change of the AgI surface area does not influence the heterogeneous freezing properties significantly.

The heterogeneous freezing temperatures for pure water on AgI reported by Aguerd et al.[23] are ~4 K lower than those in the present study. This difference may be due to a different AgI precipitation procedure, resulting in slightly different ice nucleation efficiency of the crystallites. It has been shown previously that major changes in the precipitation conditions such as the experimental protocol or large concentration variations of the Ag^+ and I^- ions as well as their concentration ratio can lead to changes in ice nucleation temperatures of up to ~10 K.[23,26] This might be due to the fact that crystallization conditions influence the AgI crystal habitus, surface charge or the number of crystal defects, and all these factors may be relevant for the ice nucleation efficiency of AgI crystals.[26,27]

Similarly, we observed changes in the ice nucleation efficiency when solutions containing NH_4^+ ions were used. In such experiments, a bimodal heterogeneous freezing peak appeared in which the onset temperature of the first maximum was some kelvins higher than the heterogeneous freezing temperature of the pure water reference case. We believe this is due to the fact that Ag^+ ions form an $[Ag(NH_3)_2]^+$ complex in ammoniated solutions. This strongly reduces the concentration of free Ag^+ ions and, hence, leads to different precipitation conditions resulting in a different ice nucleation efficiency of the AgI crystallites. Therefore, we did not include any experiments with NH_4^+ solutions to ensure that only experiments with comparable AgI crystallites were analyzed.

Emulsion Containing ATD Particles. Similar to the experiments with AgI, two freezing signals at different temperatures are observed for emulsions containing immersed ATD particles (see Figure 3b). The first (high temperature) freezing peak is attributed to heterogeneous ice freezing on the surface of ATD particles and the second (low temperature) peak to homogeneous ice freezing of droplets not containing any ATD particles. Marcolli et al.[24] have shown that the percentage of droplets containing at least one ATD particle depends on the ATD concentration of the investigated suspension. In the case of 5 wt % ATD, droplets larger than 1.5 μm in radius contain on average at least one ATD particle, and smaller ones are on average devoid of any particles. At this ATD concentration the ratio of the heterogeneous to homogeneous freezing peak area is found to be ~20:1.

3.2. Heterogeneous Freezing Temperatures as a Function of Solute Mole Fraction. Figure 4 shows the measured ice melting (T_m; panel a), heterogeneous ice freezing ($T_{f,het}$; panel b) and homogeneous ice freezing temperatures ($T_{f,hom}$; panel c) for the different IN as a function of the total solute mole fraction of the solution (x_{tot}). Here, all salts and sulfuric acid were treated as fully dissociated, whereas malonic acid was treated as undissociated. For example, an solution of $x_{NaCl} = 0.1$ results in

$$x_{tot} = (x_{Na^+} + x_{Cl^-})/(x_{Na^+} + x_{Cl^-} + x_{H_2O}) = 0.182$$

Each symbol shown in Figure 4 represents a mean value of at least two individual freezing or melting events. The ice melting temperatures of emulsions and large droplets determined with the two techniques are generally in good agreement. The ice melting temperatures (Figure 4a) decrease with increasing total solute mole fraction with a pronounced scatter at $x_{tot} > 0.075$. If these solutions were ideal, the ice melting points would not depend on the nature of the solute, but only on its mole fraction. Thus all points would fall onto a single line. However, such a behavior can be observed only in the most dilute samples, indicating the nonideality of the more concentrated solution samples.

An even larger scatter was observed in the heterogeneous ice freezing points (Figure 4b). Each IN exhibits its characteristic freezing temperature in pure water at $x_{tot} = 0$. Starting from each of these pure water values, all freezing points decrease with increasing mole fraction, whereas most series show a pronounced scatter in the freezing temperature for similar mole fractions. For example, $MgCl_2$ (light blue right-pointed triangle)

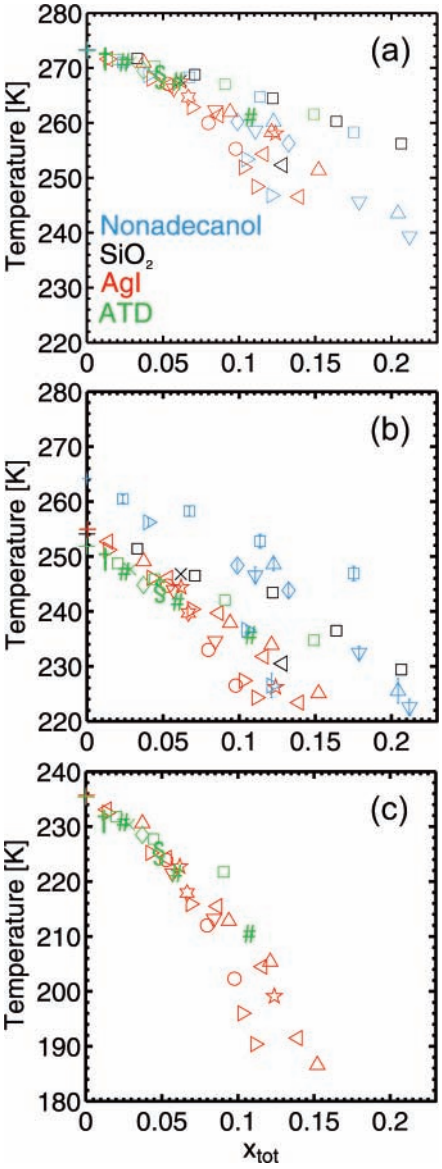

Figure 4. Ice melting temperatures (a), heterogeneous ice freezing temperatures for four different IN (b) and homogeneous ice freezing temperatures (c) of aqueous solution samples as a function of the total solute mole fraction of the solution (x_{tot}). The colors denote the different IN: light blue, nonadecanol; red, AgI; black, silica spheres; green, ATD. The mean radii of the aqueous droplets (in which the different IN were present) are approximately 1100 μm for nonadecanol, 3 μm for AgI, 1100 μm for silica and 10 μm for ATD. The symbols indicate the solutes of the investigated aqueous solutions: plus signs, H_2O; squares, $(NH_4)_2SO_4$ crosses, H_2SO_4; right-pointed triangles, $MgCl_2$; diamonds, NaCl; left-pointed triangles, LiCl; upward-pointed triangles, $Ca(NO_3)_2$; five-pointed stars, K_2CO_3; circles, CH_3COONa; downward-pointed triangles, ethylene glycol; six-pointed star, glycerol; sharp, malonic acid; dag, PEG300; paragraph sign, NaCl/malonic acid. The experimental error in x_{tot}, T_m, T_{hom} and T_{het} are less than the size of the symbols, except for T_{het} for nonadecanol. There, the uncertainty range denotes ±one standard deviation of all single freezing temperatures.

and ethylene glycol (light blue upward-triangle) solution droplets, each with x_{tot} ~0.125 and both covered by a nonadecanol monolayer, freeze at around 225 and 250 K, respectively. Figure 4c shows the homogeneous freezing points for the emulsion droplets which did not contain any AgI or ATD particles (see also Figure 3).

3.3. Role of Water Activity in Heterogeneous Ice Nucleation. So far, only few laboratory studies have provided evidence that heterogeneous ice nucleation on selected IN in the immersion mode might be described properly by water-activity-based ice nucleation theory.[11−14] In this approach it is suggested that the heterogeneous immersion ice freezing temperature of a particular IN in various aqueous solutions can be described by the solution water activity and an additional constant which is characteristic of a particular ice nucleus, but independent of the nature of the solute.

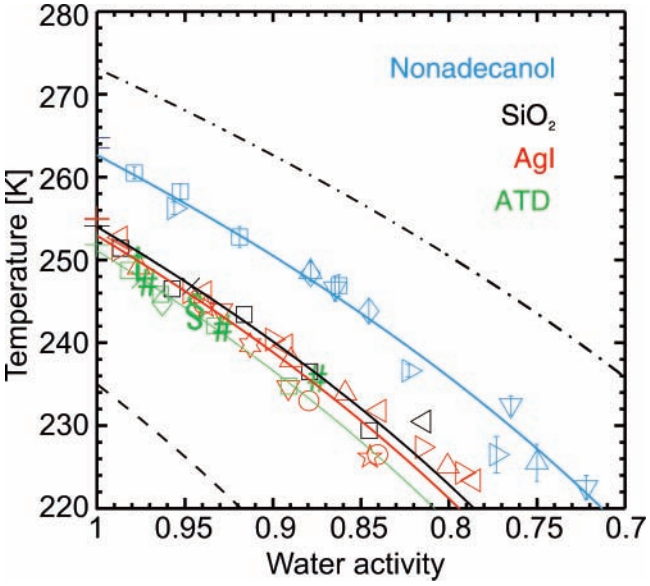

Figure 5. Heterogeneous ice freezing temperatures for four different IN as a function of the solution water activity, a_w. The same colors and symbols as in Figure 4 are used. Additionally, the dashed black line depicts the homogeneous ice freezing curve for supercooled aqueous solutions and the dash-dotted black line is the ice melting point curve.[10] The colored solid lines are horizontally shifted from the dash-dotted black line by a constant offset $\Delta a_{w,het}$, with values of 0.100 for nonadecanol, 0.173 for the silica spheres, 0.181 for AgI and 0.195 for ATD. Note that the $\Delta a_{w,het}$ values result from the particular experimental condition in this study, and that they must not be understood as universal values (see section "Ice nucleation efficiencies and atmospheric implications"). The experimental error in a_w, T_m, T_{hom} and T_{het} are less than the size of the symbols, except for T_{het} for nonadecanol. There, the uncertainty range denotes ±one standard deviation of all single freezing temperatures.

To this end we show in Figure 5 the heterogeneous freezing points of all IN as a function of the solution water activity (a_w; see Appendix B for a detailed consideration of a_w at supercooled temperatures). The heterogeneous freezing points generally decrease with decreasing a_w of the solution. The most striking result of this procedure is that the scatter in the heterogeneous freezing temperatures is significantly reduced when compared to Figure 4b: The maximum difference in freezing temperature for two data points with similar x_{tot} is roughly 25 K but is less than 8 K when the data are analyzed as a function of a_w. Moreover, the freezing points of solutions containing the same IN all accumulate around curves that are horizontally shifted from the ice melting point curve by a constant offset (see colored lines in Figure 5). The constant offset $\Delta a_{w,het}$ shown in Figure 5 were obtained by first calculating the offset for each individual measured heterogeneous freezing point to the ice melting point line:[13]

$$\Delta a_{w,het}(T_{f,het}) = a_w(T_{f,het}) - a_w^i(T_{f,het}) \quad (1)$$

Here, $a_w(T_{f,het})$ and $a_w^i(T_{f,het})$ are the water activities at the heterogeneous ice freezing temperature and on the ice melting

TABLE 1: Summary of the Ice Freezing Experiments of Droplets Covered by a Nonadecanol Monolayer[a]

solute	C_{sol} [wt %]	x_{tot}	n	N_f	$T_{f,het}$ [K]	T_m [K]	a_w
H_2O	0.0	0.0000	12	48	264.2	273.3 (273.15)[36]	1.0026
$(NH_4)_2SO_4$	5.6	0.0236	12	66	260.5	271.0 (271.4)[36]	0.9787
$(NH_4)_2SO_4$	15.0	0.0672	12	66	258.3	268.3 (268.6)[36]	0.9525
$(NH_4)_2SO_4$	23.9	0.1138	12	48	252.8	264.7 (265.1)[36]	0.9189
$(NH_4)_2SO_4$	34.2	0.1753	16	56	246.9	258.3 (259.0)[36]	0.8625
$MgCl_2$	6.9	0.0403	6	24	256.2	268.7 (268.6)[37]	0.9561
$MgCl_2$	17.1	0.1049	6	24	236.6	253.4 (253.1)[37]	0.8227
$MgCl_2$	19.6	0.1213	1	4	226.5	246.8 (246.7)[37]	0.7730
NaCl	15.1	0.0989	6	24	248.4	260.2 (261.9)[38]	0.8786
NaCl	19.9	0.1325	6	24	243.8	256.3 (256.3)[38]	0.8455
$Ca(NO_3)_2$	29.8	0.1226	6	24	248.6	260.2 (259.8)[39]	0.8786
$Ca(NO_3)_2$	43.8	0.2044	10	35	225.5	243.5 (241.6)[39]	0.7500
ethylene glycol	30.0	0.1106	6	24	246.5	258.6 (258.8)[40]	0.8647
ethylene glycol	42.9	0.1788	5	20	232.5	245.7 (246.8)[40]	0.7648
ethylene glycol	48.1	0.2119	6	24	222.6	239.3 (240.4)[40]	0.7220

[a] All droplets have a volume of 3 μL. C_{sol} is the solute concentration and x_{tot} is the total solute mole fraction of the solution assuming that all salts are fully dissociated. n is the number of investigated droplets and N_f is the total number of measured ice freezing and ice melting points. $T_{f,het}$ is the mean value of the median freezing temperatures of each individual droplet. T_m is the mean ice melting point of all individual measurements, with literature values given in brackets. a_w has been calculated from the mean T_m.[10]

point curve at the heterogeneous freezing temperatures, respectively. The first value is determined in this study (see Appendix B) whereas the latter can be calculated according to Koop et al.[10] The mean offset value for each ice nucleus was then obtained by a least-square root averaging of the individual $\Delta a_{w,het}$ values of all measurements with a particular IN. This results in $\Delta a_{w,het}$ values of 0.100 for nonadecanol, 0.173 for silica spheres, 0.181 for AgI crystallites and 0.195 for Arizona test dust, all shown as the colored lines in Figure 5. Although almost all freezing points for nonadecanol, silica and ATD collapse onto these solid lines, the agreement is not as good for the AgI measurements. However, a delimited area of $\pm 3\%$ in a_w includes all the measured freezing points for AgI. The agreement of our data with a constant offset parametrization is similar to that in the studies by Archuleta et al.,[12] Zobrist et al.[13] and Cantrell and Robinson[14] (only for the long chain alcohols with C-atom numbers of 16 and 17) but is better than that found by Zuberi et al.[11] or for the long chain alcohols with the C-atom numbers 25 and 30 investigated by Cantrell and Robinson.[14] Some of the discrepancy between the measured freezing points and the predicted lines may be attributed to the uncertainty in determining water activities at low temperatures.

However, these remaining differences between the measured freezing points and the prediction by water-activity-based ice nucleation theory are small compared to the scatter in a concentration-based representation (Figure 4b). Hence, the results shown in Figure 5 corroborate the conclusion that the kinetically driven heterogeneous ice freezing process in the immersion mode can be properly described by thermodynamic quantities. Furthermore, the large variety of investigated solutes together with different principal types of ice nuclei studied (monolayers, ionic crystals, crystals made from covalently bound network-forming compounds, and a mixture of chemically different crystallites) strongly supports the notion of the general applicability of water-activity-based ice nucleation theory for heterogeneous ice nucleation in the immersion mode.

4. Ice Nucleation Efficiencies and Atmospheric Implications

This section provides a short comparison between the ice nucleation efficiencies of the different IN and discusses some atmospheric implications of the calculated $\Delta a_{w,het}$ values of ATD and nonadecanol.

At first sight, the results shown in Figure 5 suggest that nonadecanol is the best ice nucleus followed by silica, AgI and ATD, because $T_{f,het}$(nonadecanol) > $T_{f,het}$(silica) > $T_{f,het}$(AgI) > $T_{f,het}$(ATD) at the same a_w. Freezing occurs in the individual experiments when the nucleation rate becomes on the order of 1 min^{-1}. This nucleation rate is defined as $\omega_i(T) = A \cdot j_i(T)$, where A is the surface area of the ice nucleus and $j_i(T)$ the temperature-dependent heterogeneous ice nucleation rate coefficient. The data in Figure 5 reveal that at about 250−255 K nonadecanol exhibits the highest nucleation rate for the present experimental conditions:

$$\omega_{nonadecanol} > \omega_{silica} > \omega_{AgI} > \omega_{ATD} \quad (2)$$

However, because the surface areas A of the IN were quite different in the various experiments, the heterogeneous nucleation rate coefficients j_i are a more appropriate parameter than ω_i to rank the different IN according to their nucleation efficiency. For example, the surface area of the silica spheres suspended in a 3 μL droplet is roughly 2 cm^2, which is about a factor of 10^8 larger than that of a single AgI crystallite in an emulsion droplet. This implies that $j_{AgI} \gg j_{silica}$ despite ω_{silica} being slightly larger than ω_{AgI}. In a recent study,[19] we determined $j_{nonadecanol}$ of water droplets with a nonadecanol monolayer as a function of temperature. The results indicate that the freezing temperatures for this ice nucleus decreases much more weakly than those for other IN or homogeneous ice nucleation. In particular, the heterogeneous freezing temperature of water droplets with a nonadecanol surface area of roughly 10^{-1} cm^2 (i.e., $r \approx 1100$ μm) is more than 10 K higher than that of smaller water droplets with a nonadecanol surface area of only $\sim 10^{-4}$ cm^2. The latter surface area is still $\sim 10^4$ times larger than that of an AgI crystallite, but the droplets with such a reduced nonadecanol surface area freeze at a roughly 5 K lower temperature than emulsion droplets containing AgI crystals. This implies that in the temperature range around 250−255 K the ice nucleation efficiencies are better compared according to

$$j_{AgI} > j_{nonadecanol} > j_{silica} \quad (3)$$

and indicates that AgI is the most efficient ice nucleus followed by nonadecanol and silica. Note, because ATD is a multicomponent ice nucleus that cannot be described by one j-value, it was excluded from the nucleation rate coefficient comparison.

TABLE 2: Summary of the Freezing Experiments with 3 μL Droplets Containing Silica Spheres (Particle Mass Fraction = 0.47% of the Total Water Mass)[a]

solute	C_{sol} [wt %]	x_{tot}	$T_{f,het}$ [K]	T_m [K]	a_w
H_2O	0.0	0.0000	254.1	273.2 (273.15)[36]	1.0015
$(NH_4)_2SO_4$	7.7	0.0331	251.4	271.8 (270.8)[36]	0.9865
$(NH_4)_2SO_4$	15.7	0.0709	246.5	268.8 (268.4)[36]	0.9572
$(NH_4)_2SO_4$	25.4	0.1220	243.4	264.5 (264.4)[36]	0.9163
$(NH_4)_2SO_4$	32.7	0.1639	236.5	260.3 (260.1)[36]	0.8791
$(NH_4)_2SO_4$	39.0	0.2065	229.4	256.2 (254.9)[36]	0.8454
LiCl	14.9	0.1285	230.5	252.3 (250.0)[40]	0.8142
H_2SO_4	10.8	0.0617	246.8	267.7 (266.3)[36]	0.9464

[a] C_{sol} is the solute concentration and x_{tot} is the total solute mole fraction of the solution assuming that all salts and sulfuric acid are fully dissociated. $T_{f,het}$ is the mean of 8 individual ice freezing temperature measurements. T_m is the mean value of 6 individual ice melting points, with literature values given in brackets. a_w has been calculated from the mean T_m.[10]

In the following, the $\Delta a_{w,het}$ values for nonadecanol and ATD are discussed with respect to their atmospheric applicability. Long chain alcohols together with their corresponding fatty acids have been detected in marine and urban aerosols, with typical total concentrations for various fatty alcohols or acids (C12−C32) of $10^{-12}-10^{-9}$ g per m^{-3} of sampled air.[28,29] Popovitz-Biro et al.[16] have shown that heterogeneous ice freezing temperatures of droplets covered with a 1:1 mixture of the C28 and C30 alcohols is reduced by ~10 K when compared to the freezing temperatures of droplets covered with either a pure C28 or a pure C30 alcohol. In the same study, it was also shown that freezing temperatures of a droplet covered with a mixture of the C30 alcohol and the C30 acid decrease with increasing acid concentration. Hence, only pure long chain alcohol monolayers exhibit very high freezing efficiencies, and the heterogeneous ice nucleation temperatures are strongly reduced in the case of mixed monolayers. In the atmosphere, the formation of pure monolayers of a single long chain alcohol appears to be very unlikely. Given that even water droplets with diameters between 60−100 μm covered with a pure nonadecanol monolayer freeze at only below 250 K,[19] and considering the likely predominance of mixed monolayers in atmospheric droplets, we believe that long chain alcohols are irrelevant as IN in the atmosphere although they are very useful for systematic laboratory studies, as outlined above.

On the other hand, mineral dust is believed to be one of the most relevant tropospheric ice nucleus, also at cirrus level.[30] The ATD composition is similar to that of dust originating from deserts,[31] and thus ATD can be regarded as a proxy for natural mineral dust. Little is known about the size distribution of mineral dust particles at cirrus level. Modeling studies suggest that at lower altitudes typical particle diameters are between 0.1 and 5 μm, with a maximum in number concentration at around 0.6 μm.[32] Recently, we have shown that the ice nucleation efficiency of ATD varies strongly between different particles, implying that larger particles are better IN than smaller ones.[24] The heterogeneous ice freezing temperatures of ATD-in-water suspensions increase with increasing ATD concentration. Depending on the ATD loadings, freezing temperatures down to the onset of homogeneous ice nucleation (i.e., roughly 237 K) or up to 257 K for 20 wt % ATD suspension have been measured, leading to $\Delta a_{w,het}$ values from 0.305 to 0.148. Hence, $\Delta a_{w,het}$ for ATD obtained in this study is only valid for this particular experimental conditions and cannot be regarded as a universal value for ATD under any conditions. In the 5 wt % ATD suspension many emulsion droplets contain highly potent ATD IN, and hence, $\Delta a_{w,het} = 0.195$ is close to the upper limit of ice activation in the presence of ATD particles. On the other hand, the average ATD particles exhibit diameters of ~360 nm and (assuming also 5 wt % ATD) induce freezing in pure water droplets at roughly 240 K,[33] which corresponds to $\Delta a_{w,het} = 0.274$, a value that will be even smaller for smaller ATD particles. This comparison clearly indicates that ATD, and probably also natural mineral dusts, do not exhibit a steep ice nucleation activation over a small temperature range (or ice supersaturation), as is the case for homogeneous ice nucleation, but rather show a gradual increase over a wide temperature range. This range depends on the individual ice nucleation efficiency of each dust particle within the ATD particle distribution but hardly exceeds 257 K and has its lower limit at the homogeneous freezing temperature of pure water. Similar conclusions were reached for deposition ice nucleation on ATD dust particles.[34,35] Likewise, the individual heterogeneous freezing points in experiments with montmorillonite and kaolinite particles by Zuberi et al.[11] are distributed over a temperature range of more than 20 K, from which an averaged $\Delta a_{w,het}$ of 0.242 was obtained. This large scatter may also result from the different ice nucleation efficiencies of the individual dust particles. A size dependent $\Delta a_{w,het}$ for other silicates and metal oxides was also observed by Archuleta et al.[12] The $\Delta a_{w,het}$ values of iron oxide particles treated with H_2SO_4 decreases from 0.31 for particles with a diameter of 50 nm to 0.28 and 0.25 for diameters of 100 and 200 nm, respectively. A similar decrease was also observed for aluminum oxide and aluminum silicate both treated with H_2SO_4. In these cases, $\Delta a_{w,het}$ decreases from 0.32 to 0.25 and from 0.32 to 0.26 as the diameter increases from 100 to 200 nm, respectively. This compilation clearly indicates the complex ice nucleation behavior of silicates and oxides: the nucleation rate do not just scale with surface but seems to depend also on more specific characteristics of the surface. Therefore, $\Delta a_{w,het}$ for the IN refers exclusively to the experimental conditions of this study and cannot be regarded as universal values of these IN. To apply such knowledge to IN of another size, information about the dependence of the immersion ice nucleation rate of an IN in pure water on its surface area A is required. Once this function $j_{IN}(T,A)$ in pure water is known, the $\Delta a_{w,het}$ approach developed in this manuscript can be used to apply these rates to immersion freezing in aqueous solutions.

5. Conclusion and Outlook

Heterogeneous ice freezing experiments with one organic (nonadecanol) and three inorganic IN (silver iodide, silica and Arizona test dust) have been investigated with a DSC and a custom-made cold finger cell. All IN can be considered as IN in the immersion mode, because they are either fully immersed in droplets or located at the droplets surface.

The heterogeneous ice freezing temperatures of all IN generally decrease with increasing total solute mole fraction x_{tot}

TABLE 3: Summary of the Heterogeneous Freezing Experiments of Emulsified Aqueous Solution Samples Containing AgI Crystallites[a]

solute	C_{sol} [wt %]	x_{tot}	proc	N_f	$T_{f,het}$ [K]	$T_{f,hom}$ [K]	T_m [K]	a_w
H_2O	0.0	0.0006	a	3	255.0	235.7	273.1	0.9999
H_2O	0.0	0.0003	b	3	254.9	235.4	273.4	1.0000
LiCl	2.0	0.0140	b	2	252.7	233.1	271.6	0.9867
LiCl	7.7	0.0533	b	2	246.1	224.3	266.8	0.9387
LiCl	14.9	0.0866	a	3	239.7	215.5	261.4	0.8927
LiCl	19.9	0.1393	b	3	223.4	191.5	246.6	0.7859
LiCl	19.9	0.1161	a	3	231.8	204.5	254.3	0.8396
K_2CO_3	17.9	0.0619	b	3	244.4	222.7	267.5	0.9381
K_2CO_3	39.5	0.1240	a	5	226.2	199.1	258.1	0.8448
$Ca(NO_3)_2$	13.0	0.0373	b	3	249.1	230.6	271.0	0.9761
$Ca(NO_3)_2$	29.8	0.0941	b	3	237.9	212.8	262.0	0.8897
$Ca(NO_3)_2$	43.9	0.1213	a	2	233.9	205.4	258.3	0.8589
$Ca(NO_3)_2$	43.9	0.1522	b	3	225.1	186.6	251.4	0.8008
$MgCl_2$	3.0	0.0141	b	2	251.2	232.5	271.6	0.9876
$MgCl_2$	9.0	0.0426	b	2	246.1	225.2	268.1	0.9472
$MgCl_2$	17.1	0.0690	a	4	240.4	215.9	262.9	0.9004
$MgCl_2$	22.5	0.1114	b	2	224.3	190.4	248.4	0.7923
$MgCl_2$	25.0	0.1030	a	2	227.4	196.0	251.9	0.8153
CH_3COONa	19.5	0.0529	a	3	244.7	223.9	267.1	0.9394
CH_3COONa	28.3	0.0978	b	3	226.5	202.3	255.3	0.8405
CH_3COONa	28.3	0.0798	a	3	233.0	212.0	256.0	0.8795
glycerol	39.6	0.0667	a	2	239.7	217.9	264.7	0.9129
ethylene glycol	21.4	0.0571	b	2	243.9	221.5	266.3	0.9294
ethylene glycol	29.9	0.0843	b	3	234.6	213.2	262.3	0.8912

[a] C_{sol} is the concentration of the indicated solute in the stock solution. x_{tot} is the total solute mole fraction of the final solution, which is composed of 1.6 mL of the stock solution in addition to either 0.1 mL (proc = a) or 0.05 mL (proc = b) of each a 1.64 wt % $AgNO_3$ and a 1.61 wt % KI solution. It is assumed that all salts are fully dissociated. N_f is the total number of measured ice freezing and melting points. $T_{f,het}$, $T_{f,hom}$ and T_m are the mean heterogeneous ice freezing, mean homogeneous ice freezing and mean ice melting temperatures, respectively. a_w is the estimated water activity at $T_{f,het}$; see Appendix B.

TABLE 4: Summary of the Heterogeneous Freezing Experiments of Emulsified Aqueous Solution Samples Containing ATD Particles[a]

solute	C_{sol} [wt %]	x_{tot}	N_f	$T_{f,het}$ [K]	$T_{f,hom}$ [K]	T_m [K]	a_w
H_2O	0.0	0.0000	5	251.9	235.5 (235.2)[41]	273.2 (273.15)[36]	1.0000
$(NH_4)_2SO_4$	4.8	0.0202	4	248.8	231.8 (231.9)[41]	271.5 (271.7)[36]	0.9821
$(NH_4)_2SO_4$	10.2	0.0444	2	245.9	227.7 (228.6)[41]	270.3 (270.1)[36]	0.9639
$(NH_4)_2SO_4$	19.6	0.0906	2	242.0	221.7 (222.8)[41]	267.0 (267.0)[36]	0.9328
$(NH_4)_2SO_4$	30.0	0.1491	2	234.8	not determined[b]	261.6 (261.8)[36]	0.8815
NaCl	5.9	0.0372	4	244.8	228.5 (228.4)[38]	269.5 (269.3)[38]	0.9628
H_2SO_4	5.1	0.0285	5	247.6	230.4 (230.4)[42]	271.0 (270.8)[36]	0.9751
malonic acid	10.5	0.0199	3	247.3	230.9 (230.6)[13]	271.1 (271.1)[13]	0.9773
malonic acid	25.1	0.0548	2	241.8	221.6 (222.8)[13]	267.6 (267.8)[13]	0.9348
malonic acid	39.8	0.1027	2	235.8	210.5 (211.0)[13]	261.1 (261.9)[13]	0.8811
PEG300	11.0	0.0072	2	249.8	231.3 (231.2)[43]	272.0 (272.2)[43]	0.9830
NaCl/malonic acid	4.1/8.3	0.0433	2	244.2	225.5	268.7	0.9506

[a] C_{sol} is the solute concentration and x_{tot} is the total solute mole fraction of the solution assuming that all salts and sulfuric acid are fully dissociated, whereas malonic acid was treated as undissociated. N_f indicates the number of investigated individual freezing and melting temperatures. $T_{f,het}$, $T_{f,hom}$ and T_m are as denoted in Table 3, with literature values given in brackets. a_w is the estimated water activity at $T_{f,het}$; see Appendix B. [b] The homogeneous freezing peak was too low for a reliable evaluation. Therefore, a_w at $T_{f,het}$ was approximated by $a_w(T_{f,het}) = a_w(T_m)$ in this particular case.

in the solution. However, each individual IN series shows a large scatter in the freezing temperatures, with a maximum magnitude of ~25 K at similar x_{tot} values. In contrast, when the heterogeneous ice nucleation data are plotted as a function of the solution water activity, the scatter in each individual IN series is reduced by up to a factor of about 3. This strongly suggests that water-activity-based ice nucleation theory is applicable not only to homogeneous ice nucleation but also to heterogeneous immersion ice nucleation in aqueous solutions. Using this approach, a mean constant offset of the ice melting curve ($\Delta a_{w,het}$) was calculated for each IN. The resulting freezing curves describe the investigated freezing points extremely well, with a deviation in a_w of less than 3%. The $\Delta a_{w,het}$ values are 0.100 for nonadecanol, 0.173 for silica spheres, 0.181 for AgI crystallites and 0.195 for Arizona test dust.

However, scaling the IN surface areas of AgI, nonadecanol and silica to comparable values reveals that AgI has the largest nucleation rate coefficient at similar temperatures, indicating that it is the best ice nucleus followed by nonadecanol and silica. Because of the large variability of the ice nucleation efficiencies between ATD particles, this ice nucleus shows a gradual increase of the freezing occurrence over a wide temperature range, which is in contrast to homogeneous ice nucleation or heterogeneous ice nucleation on an uniform ice nucleus. Such a freezing behavior has to be taken into account in model simulations.[24]

Nevertheless, the results of this study clearly show that heterogeneous ice nucleation in the immersion mode can be properly described by water-activity-based nucleation theory. This means that, independently of the nature of the solutes in a liquid aerosol, its heterogeneous freezing temperature can be predicted in terms of the relative humidity of the air mass (assuming that the water in the liquid phase and in gas phase are in equilibrium) once the ice nucleation efficiency of the IN in pure water is known. However, because of the complex

physical and chemical nature of atmospheric IN surfaces, most ice nuclei can exhibit a range of ice nucleation efficiencies in pure water. This is a clear limitation for a widespread applicability of our approach as quite detailed knowledge on a particular IN is required before its effect on atmospheric ice cloud formation can be reliably modeled. Nevertheless, our approach provides a simple and physically plausible tool for such studies using microphysical box models and might even be applicable for simplified sensitivity studies in global models, as was shown in two previous studies.[9,13]

Acknowledgment. We are grateful for support by the European Commission through the integrated project SCOUT-O3 and by the Swiss National Science Foundation (SNF) in various projects.

Appendix A

Experimental Data of Heterogeneous Freezing Measurements. Table 1 summarizes the measurements of the large droplets covered by nonadecanol. Only series which do not exhibit a continuous decrease in melting temperature have been considered. The mean heterogeneous ice freezing temperature and mean ice melting temperature of a total of N_f measurements is given together with melting point data from the literature (in brackets).

Table 2 lists the heterogeneous ice freezing and ice melting points of the large droplets containing silica spheres.

Table 3 summarizes the experiments with emulsified samples containing AgI crystallites. In all measurements, the solutions contain excess K^+ and NO_3^- ions from the preparation reaction, together with the deliberately added solute. The K^+ and NO_3^- ions were also taken into account when calculating the total solute mole fraction x_{tot}.

Table 4 summarizes the measurements with immersed ATD particles. The ATD concentration is always 5 ± 0.2 wt %. The measured homogeneous ice freezing and ice melting points agree very well with literature values.

Appendix B

Water Activity in the Supercooled Region. The water activity of any aqueous solution at the ice melting point, $a_w(T_m)$, can be directly derived from the vapor pressure ratio of ice and water at T_m, because at this temperature the aqueous solution and the ice are in thermodynamic equilibrium.[10] (According to our temperature calibration, the $a_w(T_m)$ values exhibit an uncertainty of ± 0.003). However, this condition is not fulfilled at the ice nucleation temperatures. Because a_w measurements at such low temperatures are rarely available, the water activity at the homogeneous ice freezing point, $a_w(T_{f,hom})$, must be approximated. The most simple assumption is that a_w is independent of temperature, i.e., $a_w(T_{f,hom}) = a_w(T_m)$.[10] For various aqueous solutions this procedure leads to a scatter of less than 2% in a_w around the homogeneous ice freezing point line predicted by Koop et al.,[10] showing that the temperature dependence of a_w is often negligible. Water activity at the heterogeneous ice freezing point, $a_w(T_{f,het})$, can be estimated in the same way.

Recently, Zobrist et al.[13] proposed an improved procedure to estimate $a_w(T_{f,het})$ of solutions for which homogeneous freezing data are available. A change in a_w as a function of temperature can be corrected by adjusting $a_w(T_{f,hom})$ such that all measured homogeneous freezing points fall onto the water-activity-based homogeneous freezing point line. Then, $a_w(T_{f,het})$ is obtained by a linear interpolation between the water activity at the homogeneous freezing point $a_w(T_{f,hom})$ determined this way and $a_w(T_m)$.[44] In the present study, this evaluation procedure was applied to the freezing experiments with emulsions containing AgI and ATD, because these measurements provided homogeneous and heterogeneous freezing temperatures in the same experimental run. For the other IN, the simple approximation $a_w(T_{f,het}) = a_w(T_m)$ was used.

References and Notes

(1) Baker, M. B. *Science* **1997**, *276*, 1072−1078.
(2) Bowles, D. J.; Lillford, P. J.; Rees, D. A.; Shanks, I. A. *Phil. Trans. R. Soc. Lond. B* **2002**, *357*, 829−955.
(3) Pruppacher, H. R.; Klett, J. D. *Microphysics of clouds and precipitation;* Kluwer: Dordrecht, The Netherlands, 1997.
(4) Wilson, P. W.; Heneghan, A. F.; Haymet, A. D. J. *Cryobiology* **2003**, *46*, 88−98.
(5) Debenedetti, P. G. *Metastable liquids*; Princeton University Press: Princeton, NJ, 1996.
(6) Zachariassen, K. E.; Kristiansen, E. *Cryobiology* **2000**, *41*, 257−279.
(7) DeMott, P. J. Laboratory studies of cirrus cloud processes. In *Cirrus*; Lynch, D. K., Sassen, K., Starr, D. O. C., Stephens, G., Eds.; Oxford University Press: Oxford, U.K., 2002.
(8) DeMott, P. J.; Rogers, D. C; Kreidenweis, S. M. *J. Geophys. Res.* **1997**, *102*, 19575−19584.
(9) Kärcher, B.; Lohmann, U. *J. Geophys. Res.* **2003**, *108*, 4402, doi: 10.1029/2002JD003220.
(10) Koop, T.; Luo, B. P.; Tsias, A.; Peter, T. *Nature* **2000**, *406*, 611−614.
(11) Zuberi, B.; Bertram, A. K.; Cassa, C. A.; Molina, L. T.; Molina, M. J. *Geophys. Res. Lett.* **2002**, *29*, doi:10.1029/2001GL014289.
(12) Archuleta, C. M.; DeMott, P. J.; Kreidenweis, S. M. *Atmos. Chem. Phys.* **2005**, *5*, 2617−2634.
(13) Zobrist, B.; Marcolli, C.; Koop, T.; Luo, B. P.; Murphy, D. M.; Lohmann, U.; Zardini, A. A; Krieger, U. K.; Corti, T.; Cziczo, D. J.; Fueglistaler, S.; Hudson, P. K.; Thomson, D. S.; Peter, T. *Atmos. Chem. Phys.* **2006**, *6*, 3115−3129.
(14) Cantrell, W.; Robinson, C. *Geophys. Res. Lett.* **2006**, *33*, L07802, doi:10.1029/2005GL024945.
(15) Gavish, M.; Popovitz-Biro, R.; Lahav, M.; Leiserowitz, L. *Science* **1990**, *250*, 973−975.
(16) Popovitz-Biro, R.; Wang, J. L.; Majewski, J.; Shavit, E.; Leiserowitz, L.; Lahav, M. *J. Am. Chem. Soc.* **1994**, *116*, 1179−1191.
(17) Knopf, D. A. Ph.D. thesis, No. 15103, ETH Zurich, Switzerland. **2003**.
(18) Seeley, L. H.; Seidler, G. T. *J. Chem. Phys.* **2001**, *114*, 10464−10470.
(19) Zobrist, B.; Koop, T.; Luo, B. P.; Marcolli, C.; Peter, T. *J. Phys. Chem. C* **2007**, *111*, 2149−2155.
(20) Seeley, L. H. Ph.D. thesis, University of Washington, Seattle, 2001.
(21) Stöber, W.; Fink, A.; Bohn, E. *J. Colloid. Interface Sci.* **1968**, *26*, 62−69.
(22) van Helden, A. K.; Jansen, J. W.; Vrij, A. *J. Colloid. Interface Sci.* **1981**, *81*, 354−368.
(23) Aguerd, M.; Clausse, D.; Babin, L. *Cryo Lett.* **1982**, *3*, 164−171.
(24) Marcolli, C; Gedamke, S.; Peter, T.; Zobrist, B. *Atmos. Chem. Phys.* **2007**, *7*, 5081−5091.
(25) Siegel, S. *Nichtparametrische statistische Methoden*; Dietmar Klotz Verlag: Eschborn b. Frankfurt a. M., 2001.
(26) Edwards, G. R.; Evans, L. F. *Trans. Faraday Soc.* **1962**, *58*, 1649−1655.
(27) Fletcher, N. H. *J. Chem. Phys.* **1959**, *30*, 1476−1482.
(28) Gagosian, R. B.; Peltzer, E. T.; Zafiriou, O. C. *Nature* **1981**, *291*, 312−314.
(29) Stephanou, E. G. *Atmos. Environ.* **1992**, *26A*, 2821−2829.
(30) DeMott, P. J; Cziczo, D. J.; Prenni, A. J.; Murphy, D. M.; Kreidenweis, S. M.; Thomson, D. S.; Borys, R.; Rogers, D. C. *Proc. Natl. Acad. Sci.* **2003**, *100* (25), 14655−14660.
(31) Krueger, B. J; Grassian, V. H.; Cowin, J. P.; Laskin, A. *Atmos. Environ.* **2005**, *39*, 395−395.
(32) Zender, C. S.; Bain. H.; Newman, D. *J. Geophys. Res.* **2003**, *108* (D14), 4416, doi:10.1029/2002JD002775.
(33) The model by Marcolli et al.[24] was used, which indicates that such particles have active sites with contact angle values between 75° and 85°, which leads to freezing temperatures of ∼242 K and 238.0 K, respectively, whith a mean value of ∼240 K. Furthermore, a nucleation rate of 1 min^{-1} was assumed, as was the case for homogeneous ice nucleation in the Koop et al.[10] paper.

(34) Möhler, O.; Field, P. R.; Connolly, P.; Benz, S.; Saathoff, H.; Schnaiter, M.; Wagner, R.; Cotton, R.; Krämer, M.; Mangold, A.; Heymsfield, A. J. *Atmos. Chem. Phys.* **2006**, *6*, 3007−3021.

(35) Knopf, D. A.; Koop, T. *J. Geophys. Res.* **2006**, *111*, D12201, doi: 10.1029/2005JD006894.

(36) Clegg, S. L.; Brimblecombe, P.; Wexler, A. S. *J. Phys. Chem. A* **1998**, *102*, 2137−2154.

(37) Koop, T. *Bull. Chem. Soc. Jpn.* **2002**, *75*, 2587−2588.

(38) Rasmussen, D. H.; MacKenzie, A. P. *Water structure at the water polymer interface*; Jellinek, H. H. G., Ed.; Plenum Press, New York, 1972; pp 126−145.

(39) Angell, C. A.; Sare, E. J.; Donella, J.; MacFarlane, D. R. *J. Phys. Chem.* **1981**, *85*, 1461−1464.

(40) Lide, D. R. *Handbook of chemistry and physics*, 79th ed.; CRC Press: New York, 1998.

(41) Bertram, A. K.; Koop, T.; Molina, L. T.; Molina, M. J. *J. Phys. Chem. A* **2000**, *104*, 584−588.

(42) Koop, T.; Ng, H. P.; Molina, L. T.; Molina, M. J. *J. Phys. Chem. A* **1998**, *102*, 8924−8931.

(43) Zobrist, B.; Weers, U.; Koop, T. *J. Chem. Phys.* **2003**, *118*, 10254−10261.

(44) The linear interpolation was omitted in Zobrist et al.[13], because of the small difference between the homogeneous and heterogeneous freezing temperatures.